Computational Modeling Predicts Interleukin-10 Control of Lesion Sterilization By Balancing Early Host-Immunity-Mediated Antimicrobial Responses With Caseation During *Mycobacterium tuberculosis* Infection

Nicholas A. Cilfone[*], **Christopher B. Ford**[†], **Simeone Marino**[‡], **Joshua T. Mattila**[§], **Hannah P. Gideon**[§], **JoAnne L. Flynn**[§], **Denise E. Kirschner**[‡], and **Jennifer J. Linderman**[*]

[*]Department of Chemical Engineering, University of Michigan, Ann Arbor, MI, USA

[†]Broad Institute of MIT & Harvard, Cambridge, MA, USA

[‡]Department of Microbiology and Immunology, University of Michigan Medical School, Ann Arbor, MI, USA

[§]Department of Microbiology and Molecular Genetics, University of Pittsburgh School of Medicine, Pittsburgh, PA, USA

Abstract

Although almost a third of the world's population is infected with the bacterial pathogen *Mycobacterium tuberculosis* (*Mtb*), our understanding of the functions of many immune factors involved in fighting infection is limited. Determining the role of the immunosuppressive cytokine interleukin-10 (IL-10) at the level of the granuloma has proven difficult due to lesional heterogeneity and the limitations of animal models. Here we take an *in silico* approach and, through a series of virtual experiments, we predict several novel roles for IL-10 in TB granulomas: (1) decreased levels of IL-10 lead to increased numbers of sterile lesions, but at the cost of early increased caseation, (2) small increases in early antimicrobial activity cause this increased lesion sterility, (3) IL-10 produced by activated macrophages is a major mediator of early antimicrobial activity and early host-induced caseation and (4) increasing levels of infected macrophage derived IL-10 promotes bacterial persistence by limiting the early antimicrobial response and preventing lesion sterilization. Our findings, currently only accessible using an *in silico* approach, suggest that IL-10 at the individual granuloma scale is a critical regulator of lesion outcome. These predictions suggest IL-10 related mechanisms that could be used as adjunctive therapies during TB.

Introduction

Tuberculosis (TB), a deadly infectious disease caused by the bacterium *Mycobacterium tuberculosis* (*Mtb*), results in 1–2 million deaths per year (1). Control of the TB epidemic is limited by a complicated drug regimen, development of antibiotic resistance, and the lack of

Corresponding Author: Jennifer J. Linderman, Department of Chemical Engineering, University of Michigan, 2300 Hayward St., 3074 H.H. Dow Building, Ann Arbor, MI, 48109, USA, Phone: 734-763-0679, linderma@umich.edu.

an effective vaccine against infection and disease. Understanding the complex host response to *Mtb* is essential for developing new and improved strategies to fight infection. Granulomas, organized collections of immune cells and bacteria that form in lungs and other organs, are an essential feature of the immune response to *Mtb* and serve as the central site of host-pathogen interaction. Cytokines are critical to coordinating an effective yet controlled immune response to *Mtb* within a granuloma. Human and animal models have demonstrated that the pro-inflammatory cytokines tumor necrosis factor-α (TNF) and interferon-γ (IFN-γ) are essential to the host-response against *Mtb*; however, other cytokines also participate in the response (1–3). Our focus here is on the anti-inflammatory cytokine interleukin-10 (IL-10), whose role in *Mtb* infection remains unclear.

IL-10 functions by inhibiting cytokine/chemokine production, preventing cellular apoptosis/necrosis, and altering macrophage activation phenotype (2, 4–6). IL-10 is produced by a spectrum of immune cells during infection, including macrophages, T-cells, and neutrophils (7). Macrophages are a primary source of IL-10 during *Mtb* infection, and activated macrophage derived IL-10 may function to limit host-induced tissue damage (2, 8–10). *Mtb*-infected macrophages produce IL-10 when toll-like receptors and other pattern recognition receptors interact with *Mtb*-derived lipids and other molecules (1, 11–16). HN-878 and CH strains of *Mtb* induce greater production of IL-10 from macrophages than the lab strain H37Rv, and thus may be linked to increased pathogen virulence (1). T cells, including CD4+, CD8+, and regulatory T cells, can also produce large quantities of IL-10 and may contribute to control of immunity (17–22). However, these cells can co-produce pro- and anti-inflammatory cytokines. For instance, CD4+ T cell clones from human bronchoalveolar lavage fluid with active TB primarily produced interferon-γ and IL-10 upon re-stimulation (23, 24). Recently, neutrophils have been identified as a source of IL-10, although production rates *in vivo* are uncharacterized; studies have shown neutrophils can produce IL-10 when stimulated with *Mtb* antigens, but can also function to stimulate IL-10 production from macrophages (25–27). Due to the spectrum of cellular sources it has been difficult to determine in experimental systems the primary sources of IL-10 in a granuloma and its main functional role.

IL-10 may dampen the strength of the immune response to *Mtb*, minimizing lung damage and pathology (1, 7, 8, 28). A central feature of many TB granulomas is an acellular core of caseous necrosis (3, 29). Caseous necrosis provides the opportunity for airway erosion and can lead to calcification and fibrosis of lesions, both highly damaging to host lung tissue (29). However, caseation can also lead to a low oxygen environment that is limiting to Mtb replication (30). Both host-immunity and pathogenic mechanisms, including *Mtb*-induced macrophage bursting, TNFR1-induced apoptosis/necrosis, Fas ligand-induced cell death, perforin/granulysin from cytotoxic T cells, reactive nitrogen/oxygen species (RNS and ROS) produced within macrophages, and neutrophil infiltration and death can contribute to caseous necrosis. However, the contribution of neutrophils to outcome at the individual granuloma scale, particularly for primate granulomas, remains incomplete (29, 31–36). IL-10 has been shown to limit macrophage apoptosis/necrosis in the context of *Mtb* infection, but how that translates to prevention of caseation is still unclear (6, 29, 31, 34, 36–44).

Most *in vivo* investigations into the role of IL-10 during *Mtb* infection have been performed in murine models. However, studies using *Il10*$^{-/-}$ mice have shown contradicting results. Initial reports demonstrated no difference in bacterial load, while more recent studies have shown increased inflammatory responses and reduced bacterial burdens in both lungs and spleen (1, 45, 46). Additionally, some reports indicated reduction in bacterial load was associated with increased pathology and inflammatory cytokine production (28). Transgenic mice that overexpress IL-10 have significantly higher bacterial loads that normal mice (47, 48). Abrogation of IL-10 signaling in the CBA/J murine model using anti-IL-10R antibodies reduced bacterial burdens in the lungs and enhanced host inflammatory-responses (1, 45). Taken together, these results lend insight into the role of IL-10 during the immune response to *Mtb*, however murine models of TB lack many characteristics of human lesions, including the ability to recapitulate a truly latent state of infection, characteristics of granuloma organization including caseation, and the spectrum of cell types producing IL-10 (49–51). The murine model of *Mtb* infection is progressive with bacterial levels and dynamics inconsistent with human and non-human primate infections (52). Therefore, conclusions drawn about the influence of IL-10 on bacterial load in the murine model may not be reflective of TB in humans and need to be further tested. In addition, studies of the effects of IL-10 on bacterial loads at a single granuloma scale have not been performed in the murine model of TB.

The non-human primate (NHP) model recapitulates the course and character of human TB disease. Recent studies in the NHP model of *Mtb* infection have indicated large variability among lesions within a single host; however, we have a limited understanding of what host factors (such as IL-10 levels) drive the observed variability (52). Genomes (chromosomal equivalents, or CEQ, i.e. total chromosomal DNA in lesions) from non-viable *Mtb* degrade very slowly in lesions (estimated at maximum of ~4% per day), and thus measuring CEQ using PCR on a housekeeping gene provides an estimate of total bacterial burden (both viable and dead bacteria) in a lesion. The ratio of colony-forming units (CFU, i.e. viable bacteria) to CEQ reflects antimicrobial activity at the individual lesion scale (52). In lesions from macaques with either active or latent infection, the killing capacity of the immune response is similar at the individual granuloma scale, with a significant number of sterile lesions (a lesion with no detectable bacteria) existing in both outcomes. This heterogeneity at the lesional scale makes it difficult to identify predictors of disease outcome, but is critical to recapitulating the immune response in humans.

Although the NHP model of TB is the most representative experimental model of human TB, studies investigating the role of IL-10 during *Mtb* infection have not yet been reported. Thus, additional work is needed to elaborate the role of IL-10 and mechanisms of its action during *Mtb* infection. Therefore, we use an *in silico* approach to investigate the role of IL-10 in controlling antimicrobial activity, lesional sterility, and caseation during *Mtb* infection. We utilize our hybrid agent-based model (*GranSim*), which includes IL-10 receptor-ligand scale dynamics, to predict mechanisms regarding how IL-10 dynamics control infection outcome at the individual granuloma scale (8). We first update and validate *GranSim* based on new data on CFU trajectories from the NHP model of TB (52). We then use *GranSim* to probe the role of IL-10 at the individual granuloma scale by performing virtual IL-10

knockouts, temporal virtual IL-10 knockouts, cell-specific IL-10 knockouts, and perturbations of IL-10 production rates. We ask: (1) What are the effects of IL-10 at the level of a single granuloma and do they change over time? (2) Does IL-10 have a significant affect on bacterial burden, likelihood of lesion sterilization, or caseation levels? (3) Which cells are the primary sources of IL-10 in a granuloma? (4) Do *Mtb* strains that induce greater IL-10 production prevent antimicrobial activity?

Methods

Overview

We recently developed a new version of *GranSim*, a hybrid agent-based model (ABM) of *Mtb* infection, that incorporates IL-10 and TNF dynamics across multiple temporal and spatial scales (8, 53, 54). We are now able to calibrate our model with new data derived from an NHP model of TB infection on CFU per lesion (52, 55–57). We subsequently validate the model by comparing model predictions of bacterial doubling time against measured values in the NHP model and perform virtual deletions (TNF and IFN-γ) of previously identified essential mediators (52, 58, 59). As this model now incorporates detailed descriptions of both IL-10/IL-10R and TNF/TNFR-associated molecular interactions and a representation of *Mtb* dynamics similar to humans, it is poised to predict the role of IL-10 and mechanisms driving its effects at a single granuloma scale. We perform *virtual experiments* that are currently difficult or infeasible in animal models of TB, including cessation of IL-10 production from individual and specific cell types and tracking the temporal dynamics of sterile lesions. Furthermore, we explore the effects of increased production of IL-10 derived from infected macrophages. Details for these virtual experiments are given below.

Hybrid Multi-Scale Agent Based Model of Mtb Infection

Our multi-scale ABM of *Mtb* infection, *GranSim*, describes immune processes over three different scales: tissue, cellular, and molecular (8, 53, 54). Briefly, at the tissue and cellular scale, *GranSim* includes macrophages and T-cells (agents), each with multiple states. Macrophages can be resting, infected, chronically infected, or activated macrophages, and T-cells can be pro-inflammatory, cytotoxic, or regulatory. Included in the model are three bacterial sub-populations: intracellular *Mtb*, extracellular *Mtb*, and non-replicating *Mtb*. The agents and bacterial population interactions are described by a well-defined set of rules and interactions between immune cells and *Mtb* in the lung and can be found in (8, 53, 54). At the molecular scale we capture receptor-ligand binding and trafficking, as well as the secretion, diffusion, and degradation of the cytokines IL-10 and TNF. We assume IL-10 and TNF binding and internalization directly modulate cellular processes, such as down regulation of TNF production (see (8) for a full model description). We model the cellular sources of IL-10 as: infected macrophages, activated macrophages, and a proportion of effector and cytotoxic and regulatory T-cells. As the functionality of neutrophils is still unclear and the production rate of IL-10 still uncharacterized we do not explicitly model neutrophil IL-10 production (25–27). We link molecular scale events to cellular and tissue scale events by allowing dynamics within each scale to influence behavior on other scales (e.g. TNF-induced apoptosis/necrosis) (8). The ABM is two dimensional (2D) and

represents a 4 mm^2 cross-section of lung tissue. Infecting a single macrophage with *Mtb* leads to the development of ~1 mm diameter lesions, which falls into the range of individual granuloma sizes observed in the NHP model (1–5mm) of TB (55, 57). The ABM can reproduce larger lesion sizes by simulating a larger cross-section of lung tissue (e.g. 16 mm^2) (unpublished data). A key feature of our ABM is the flexibility to include data as they become available; therefore we update some *GranSim* rules to better reflect current biological knowledge of the immune response to *Mtb* (Supplemental Table I).

Non-Human Primate Infection, Classification, CFU, and CEQ

In previously published work (52, 55–57), 32 healthy cynomolgus macaques (*Macaca fascicularis*) were infected with ~25 CFU of the Erdman strain of *Mycobacterium tuberculosis* via bronchoscopic instillation. Lesions were excised at various time points (between 26 and 296 days post-infection) where bacterial burden and chromosomal equivalents were measured (Supplemental Table I). Bacterial burden was measured by enumeration of colonies (CFU) after 3 weeks of culture on 7H10 agar. Sterile lesions were defined as lesions with no detectable colonies after 6 weeks of culture (see (52) for justification). Chromosomal equivalents (CEQ) were measured by real-time quantitative PCR of isolated *Mtb* genomic DNA from lesions. Full descriptions of NHP infection and data collection methods, as well as the data used in this study, can be found in (52, 55–57).

Calculation of CFU and CEQ

The sum of intracellular *Mtb*, extracellular *Mtb*, and non-replicating *Mtb* is the total bacterial burden, and is comparable to CFU in the NHP model of *Mtb* infection. Thus, we refer to all total bacterial burden measurements generated by *GranSim* as CFU. Since CFU data collected in the NHP model of TB are from whole lesions, we scale our 2D model-generated CFU results to 3D to allow for direct comparison. For the scaling, we calculate the minimum radius of a granuloma sphere that encompasses the entire CFU population and determine an appropriate 2D to 3D scaling factor. Scaled CFU data is only shown when comparing to NHP data. We measure CEQ in *GranSim* by tracking each bacterial division. For simplicity, we assume no degradation of CEQ in the lesion (52). The ratio CFU/CEQ reflects the degree of killing, with smaller values reflecting a more efficient bactericidal response.

Calculated Measures of Inflammation and Tissue Damage

In this work, we report *TNF concentration* (pg/mL) as a general biomarker of inflammation in a granuloma. We calculate average TNF concentrations by summing soluble TNF in all compartments contained within the lesion and converting to a concentration using the volume of a 2D grid compartment (assuming a uniform depth of the 2D simulation environment of one compartment; similar to a planar sheet). *GranSim measures caseous necrosis as a proxy for tissue damage* by monitoring levels of infected macrophage bursting, Fas/FasL killing by T cells, perforin/granulysin killing by cytotoxic T cells, activated macrophage death (high levels of ROS/RNS), and TNF-induced apoptosis/necrosis within each grid compartment. *GranSim* considers TNF-induced apoptosis/necrosis to be a general process of induced cell-death and does not differentiate between apoptosis, necrosis, necroptosis, or apoptotic necrosis, thus TNF-induced cell death contributes to caseous

necrosis (29, 31). Although this is not a perfect measure of tissue damage, caseous necrosis results as a consequence of infection and inflammation can be detrimental to host tissues. A grid compartment is classified as caseous necrotic when the number of aforementioned events passes a threshold defined by a model parameter (Supplemental Table I), the idea being that after a certain number of these events occur, the tissue in that compartment is likely to become caseous necrotic (8, 53, 54). We also use two previously established measures by our group to examine tissue damage: the ratio of infected macrophage apoptosis/necrosis to healthy macrophage apoptosis/necrosis, $R_{apoptosis}$, and a modified version of the *Host-Pathogen Index* (H.P.I), which is a combined metric of CFU and healthy macrophage apoptosis/necrosis scaled between zero and one (8, 54). These latter measures are examined fully in the Supplementary Figures.

Calculation of Instantaneous Mtb Doubling Time

We calculate an instantaneous doubling time of *Mtb* by assuming that during the first 20 days of infection bacteria are able to replicate freely following an exponential growth curve (52). Thus, the instantaneous doubling time (t_d) is calculated by:

$$t_d = \frac{\ln(2)}{\ln(CEQ(t))}t \quad (1)$$

Here, t is the time point of interest post-infection and CEQ(t) is the CEQ at the time point of interest post-infection. Comparisons of doubling times beyond the onset of the adaptive immunity (~25–35 days post-infection) cannot be drawn since the CFU and CEQ curves do not follow classical exponential growth due to host bactericidal processes (52).

Classification of Lesions

We classify simulated lesions at 200 days post-infection into 2 outcomes at the granuloma scale: *sterile lesions*, and *non-sterile lesions* (60). *Non-sterile lesions* are defined as lesions that have a non-zero CFU at 200 days post-infection. *Non-sterile lesions* can be split into two types: *controlled growth* or *uncontrolled growth*. *Controlled growth* is defined as robust control of *Mtb* within a lesion with CFU ($<10^4$ CFU) levels comparable to lesions in the NHP model of TB (52, 55, 61, 62). *Uncontrolled growth* is defined by an immune response incapable of limiting the growth of *Mtb* in a lesion. In the NHP model of TB, this corresponds to lesions that either split into multiple lesions or disseminate. The pathogen is able to replicate freely and the CFU is well above levels in the *controlled growth* outcome ($>10^4$ CFU). *Sterile lesions* are defined as the complete removal of live *Mtb* in the lesion (zero CFU) at any time post inoculum. The classification of a lesion at day 200 is used for any previous time points where data is separated by outcome (e.g., a lesion that becomes sterile at day 150 is always counted in the sterile category).

Virtual Deletion of IL-10 (Complete Il10$^{-/-}$)

It has been shown *in vivo* that there are multiple cellular sources of IL-10 in primates, therefore we included in the model the following cell types producing IL-10: infected macrophages, chronically infected macrophages, activated macrophages, and regulatory T-

cells (8). We simulate virtual IL-10 deletions that mimic an experimental *Il10⁻/⁻* phenotype by setting IL-10 synthesis by all cell-types to zero at the beginning of a simulation and simulating 200 days of infection. We report: CFU/lesion at 200 days post-infection, CFU/CEQ at 25, 50, 100, and 200 days post-infection, TNF concentrations at 25, 35, 45, 55, 100, and 200 days post-infection, and caseous necrosis per lesion at 25, 35, 45, 55, 100, and 200 days post-infection. In addition, we perform IL-10 knockouts after lesions form in response to *Mtb* by setting IL-10 synthesis by all cell-types to zero at 25, 50, 75, and 100 days post-infection. An advantage of our *in silico* approach is that we can analyze sterile granulomas from WT simulations compared to sterile granulomas from IL-10 deletion simulations. We report the fraction of infected macrophages that undergo induced cell-death, fraction of resting macrophages that become NFκB activated, the number of macrophages that have been exposed to *Mtb*, and CFU/lesion at day 45 post-infection. We then create an IL-10 deletion parameter set that has reduced rates of NFκB activation and TNF-induced apoptosis (termed IL-10 K/O Low Apop/Act) in order to determine the mechanisms underlying processes leading to lesion sterilization.

Virtual Transgenic IL-10

We perform virtual IL-10 transgenic experiments by increasing or decreasing the IL-10 production rate of each cellular source of IL-10 individually. Rates from 1/5 to 5 times the normal production rate are tested, with production from all cell types changed by the same factor. We then simulate 200 days of infection post inoculum. We report CFU/lesion and CFU/CEQ at 200 days post-infection, while TNF concentrations are reported at 35 days post-infection and the number of caseous necrosis compartments per lesion is reported at 50 days post-infection. In addition, we calculate the fraction of bacterial populations (intracellular, extracellular, non-replicating) in non-sterile granulomas at 200 days post-infection. We chose these time points of interest based on insights we derived from the virtual deletion of IL-10.

Virtual Deletion of Cell-Specific IL-10 Sources

We perform virtual IL-10 deletions of specific cellular sources by setting IL-10 production from those cells to zero at the beginning of a simulation. Three cell-specific IL-10 deletions are examined: infected macrophage *Il10⁻/⁻* (combined deletion of infected macrophages and chronically infected macrophages), activated macrophage *Il10⁻/⁻*, and regulatory T-cell *Il10⁻/⁻*. We then simulate 200 days of infection post inoculum. We report: CFU/lesion at 200 days post-infection, CFU/CEQ at 25, 50, 100, and 200 days post-infection, TNF concentrations at 50 and 100 days post-infection, and caseous necrosis per lesion at 50 and 100 days post-infection.

Virtual Variability in Mtb Strain Induced IL-10

Multiple clonal lineages of *Mtb* have evolved over the long course of its existence (13). Each of these lineages has significant inter-strain variability in levels of induction of IL-10 in macrophages (11–15). In our model, when a macrophage becomes infected with *Mtb* it begins synthesizing IL-10 at a specific rate. We modulate the synthesis rate of IL-10 from infected macrophages (10-fold reduction to 1000-fold increase from its baseline level),

while keeping the rates of IL-10 synthesis from activated macrophages and regulatory T cells identical (at baseline rates). In addition, this allows us to also explore indirectly the effects of neutrophils as they have been shown to increase production of IL-10 from infected macrophages (25–27). We then simulate 200 days of infection post inoculum. Changes in infected macrophage IL-10 synthesis rate are reflected in the fractional synthesis rate (f_{Mi}), which is defined as:

$$f_{Mi} = \frac{r_{Mi}}{r_{Mi} + r_{Ma} + r_{Tr}} \quad (2)$$

Here, r_{Mi} is the infected macrophage IL-10 synthesis rate, r_{Ma} is the activated macrophage IL-10 synthesis rate, and r_{Tr} is the regulatory T cell IL-10 synthesis rate. We report: percentage of IL-10 derived from infected macrophages, CFU/lesion, CFU/CEQ, number of activated macrophages, and number of infected macrophages at 200 days post-infection.

Uncertainty and Sensitivity Analysis

Uncertainty and sensitivity analysis is used to identify IL-10 model parameters that have significant effects on model outputs. We use Latin hypercube sampling (LHS) to simultaneously vary multiple model parameters and sample the parameter space (63). Partial rank correlation coefficients (PRCCs) quantify the effects of varying each parameter on non-linear outputs, where a PRCC of −1 represents a perfect negative correlation and a PRCC of +1 represents a perfect positive correlation. PRCCs are differentiated based on a students t-test to indicate significance. In this work we generate 250 unique parameter sets, each of which are replicated four times, yielding 1000 simulations. Average values of model outputs (e.g. CFU, CFU/CEQ) are used to calculate PRCC and p-values.

Computational Platform

Our ABM is constructed using the C++ programming language, Boost libraries (distributed under the Boost Software License – www.boost.org), and the Qt framework for visualization (distributed under GPL – www.qt.digia.com). The ABM is cross-platform (Macintosh, Windows, Unix) and can be run with or without our visualization software. Simulations were performed on the Flux computing cluster, provided by Advanced Research Computing at the University of Michigan, and OS X based multi-core personal computers (Intel Quad Core i7 Apple Macbook Pro). Data manipulation was carried out in MATLAB R2012a (Natick, MA). Plots and statistical tests were created using GraphPad Prism 6 (La Jolla, CA).

Results

Model Calibration and Validation with Non-Human Primate (NHP) Data

We first calibrate our model with new CFU per lesion data from the NHP model of TB. We utilize a data set derived from 32 NHPs in which CFU per lesion data has been collected between 28 and 296 days post-infection (52, 55–57, 62). Each NHP has 3–37 lesions with non-sterile lesions containing ~10 to ~10^6 CFU per lesion. We re-calibrated our previously published version of *GranSim*, by varying multiple model parameters (Supplemental Table

I) in order to best fit the temporal median CFU per lesion data (8). Sterile lesions were excluded from both the NHP-derived data set and the model-generated data set during model calibration of median CFU to minimize effects on median CFU of non-sterile lesions. We identify a baseline parameter set (hereafter noted as the wild type, WT, parameter set) that replicates the peak median NHP CFU per lesion data at day 28 and leads to robust control of median CFU per lesion beyond 100 days post-infection (Fig. 1A, 1C). The percentage of model-generated sterile lesions at 200 days post-infection (~15–30%, N=100) is consistent with the number of sterile lesions observed in NHPs (~33%, N=476) (52). Simulated lesions are able to recapitulate histological observations from NHP lesions, wherein infected macrophages and caseation that are located primarily in the core of the lesion are surrounded by an outer cuff of healthy macrophages and a peripheral cuff predominantly comprised of lymphocytes (55, 64, 65). The cellular spatial configuration of the lesion is emergent behavior that arises as a consequence of the model rules.

We validate our WT parameter set against two data sets: (1) instantaneous bacterial doubling times calculated from CEQ in the NHP model of TB and (2) deletion of TNF and IFN-γ. Comparison of instantaneous *Mtb* doubling times between simulated (Eqn. 1) and NHP lesions show good agreement, with the median simulated doubling times falling within the min-max range of NHP doubling times for both 10 and 20 days post-infection (Table I) (52). We then simulate virtual deletions of TNF and IFN-γ at the initialization of infection. Observations in the NHP and murine models of TB have indicated that removal of TNF causes lesions to function poorly, leading to elevated bacterial loads and dissemination (58, 66). Similarly, removal of IFN-γ causes extensive tissue damage with an immune response that is unable to restrict bacterial growth (59). TNF and IFN-γ virtual deletions show an approximately 1000-fold increased in median CFU per lesion (Fig. 1B) with large, disseminating lesions in the TNF deletion (Fig. 1D) and extensive tissue damage in the IFN-γ deletion (Fig. 1E). These simulations mark the first time a computational model of *Mtb* infection has been calibrated and validated with temporal CFU data and apparent *Mtb* doubling times from the NHP model, a model with bacterial dynamics and clinical classifications comparable to human *Mtb* infection (52, 55, 64). We are now in a unique position to use our model to predict the role of IL-10 in modulating antimicrobial activity, host-induced caseation, and lesion sterility.

Prediction 1: Reduced Bacterial Loads in Simulated IL-10 Knockouts are Due to Increased Sterilization of Lesions

In order to understand the role of IL-10 during *Mtb* infection at the individual granuloma scale, we simulated a virtual IL-10 deletion (referred to as IL-10 K/O) at the initialization of infection. We analyze model outputs for differing virtual lesion outcomes (sterile vs. non-sterile) in both WT and IL-10 K/O lesions to better understand factors driving infection outcome. Strikingly, we observed an ~2-fold increase in the number of sterile lesions in the simulated IL-10K/O as compared to WT (Fig. 2A). Mean CFU per lesion at day 200 was reduced ~1.75-fold when both sterile and non-sterile lesions are considered together; however, mean CFU per lesion was unchanged in IL-10 K/O non-sterile lesions compared to WT non-sterile lesions. Therefore, we predict that reduced CFU in the virtual IL-10 K/O is due to an increased number of sterile lesions and not a reduction in CFU in every lesion. The

frequency of sterilization of individual granulomas is likely a determining factor in infection outcome (active vs. latent TB) therefore IL-10 may be a key regulator of clinical outcome.

We next simulated virtual IL-10 deletions beginning at days 25, 50, 75, and 100 post-infection. We observed a transient increase in the number of sterile lesions (Fig. 2B) with a 7-fold increase when IL-10 is removed at day 25 post-infection and smaller increase in sterile lesions when IL-10 was deleted at later time points. Thus, the predicted increase in sterile lesions upon deletion of IL-10 is a transient phenomenon that mainly occurs during the early immune response to *Mtb*.

Prediction 2: IL-10 Controls the Early Immune Response to Mtb at a Lesional Scale

To better understand the role of IL-10 during the early immune response, we examined simulated lesions up to 200 days post infection. Peak CFU ($\sim 10^3$-10^4) and CEQ ($\sim 10^4$) were comparable between simulated WT and IL-10 K/O lesions, occurring 4 weeks post-infection (Supplemental Fig. S1). Mean CFU/CEQ is ~2-fold lower for simulated IL-10 K/O lesions at days 50, 100, and 200 post infection, indicating increased antimicrobial activity (Supplemental Fig. S1). However, when sterile and non-sterile simulated IL-10 K/O lesions are analyzed separately, it becomes apparent that the observed increase in antimicrobial activity is transient in both populations. Sterile lesions and non-sterile lesions have lower CFU/CEQ at day 50, compared to WT lesions (~4-fold vs. ~1.75-fold) with no differences in CFU/CEQ levels in non-sterile lesions after day 50 (Fig. 2C). In simulated IL-10 KOs, increased antimicrobial activity is coupled to an increased early inflammatory response and increased caseation, with elevated levels of TNF at days 35 and 45 (Fig. 2D) and an ~1.2–1.5-fold increase in caseous necrosis at day 45 and 55 (Fig. 2E). These results indicate that increases in antimicrobial activity due to virtual IL-10 deletion occur mainly during the early immune response, helping promote sterilization at the cost of early caesous necrosis. As infection progresses, the levels of caseous necrosis stabilize as healing and tissue remodeling can occur. Total CFU in the lesion declines to significantly lower values than in the early stages of infection and less antimicrobial activity is necessary (Fig. 1B). Taken together, our simulations predict that IL-10 transiently restricts early antimicrobial activity, limiting host-inflammation-induced caseation in individual lesions and preventing lesion sterilization (Supplemental Fig. S1).

Prediction 3: Increased Sterilization of Lesions in IL-10 Deletions is a Result of Small Differences in Antimicrobial Activity of the Early Immune Response

An advantage of our computational model as compared to experimental systems is that we can track the entire time course of individual lesions. Unlike experimental systems, where it can be difficult to determine what antimicrobial processes lead to sterilization of a lesion is difficult, our model tracks how the immune response changes within a granuloma from infection initiation to sterilization. Therefore, we sought to understand what immune mechanisms contribute to the increased percentage of sterile lesions in our virtual IL-10 deletion simulations. We compared antimicrobial mechanisms (i.e. macrophage NFκB activation and induced cell-death of infected macrophages) between simulated WT and IL-10 K/O sterile lesions at 45 days post-infection, when the antimicrobial response is the strongest. In this scenario, we observe small, yet significant, differences in the fraction of

infected macrophages that undergo apoptosis (6% increase in IL-10 K/O sterile lesions) and the fraction of NFκB$^+$ macrophages present (15% increase in IL-10 K/O sterile lesions) (Fig. 3A). These small increases in antimicrobial activity limit healthy macrophage exposure to *Mtb*, which prevents the bacteria from residing in the intracellular niche where it is more difficult to kill. The mean bacterial load is significantly lower in IL-10 K/O lesions, 27 CFU vs. 48 CFU. Therefore, we predict that small increases in antimicrobial mechanisms lead to increased sterilization in IL-10 knockouts.

In order to verify that increases in antimicrobial mechanisms were causing the increased frequency of sterile lesions, we created an IL-10 KO parameter set with reduced rates of NFκB activation (decreased by 6%) and TNF-induced apoptosis (decreased by 15%). Using this parameter set, the percentage of sterile lesions at 200 days post-infection returns to WT levels (Fig. 3B). Therefore, our model predicts that the mechanism driving increased frequency of sterile lesions in the simulated IL-10 K/O is a result of small increases in antimicrobial mechanisms, which limits exposure of macrophages to bacteria (Fig. 3A), preventing infection of new macrophages and allowing activated macrophages to kill extracellular bacteria.

Prediction 4: Modulating Total IL-10 Concentrations Demonstrates Control of Antimicrobial Activity and Host-Immunity Derived Caseation

Our predictions above suggest that modulating concentrations of IL-10 might be a successful way to increase sterilization of lesions. To test this, we modulated the total concentration of IL-10 within a lesion (see Methods). An advantage of our modeling approach is the ability to finely control levels of IL-10 in lesions, which proves difficult in experimental systems. We perform virtual transgenic simulations by increasing or decreasing the synthesis rate of IL-10 simultaneously in all cell populations (5-fold reduction to 5-fold increase in small increments). A 5-fold increase in total IL-10 production rate increases the mean CFU per lesion at day 200 from ~300 to ~10,000 (shifting lesion classification from *controlled growth* to *uncontrolled growth*), while a 5-fold decrease in IL-10 production rate decreases the mean CFU per lesion to ~50 (Fig. 4A). As IL-10 production increases, no sterile lesions are observed; decreasing total IL-10 production leads to an eventual ~9-fold increase in the number of sterile lesions (chi-squared trend test, p<0.0001) (Fig. 4A). CFU/CEQ at day 200 is correlated with IL-10 levels (Fig. 4B), while levels of TNF at day 35 (Fig. 4C) and caseous necrosis at day 50 (Fig. 4D) are inversely correlated with IL-10 levels.

We also predict that changing levels of IL-10 production induces bacterial populations to change within lesions that do not sterilize (Fig. 4E). At 200 days post-infection, non-sterile lesions with reduced IL-10 production have increased caseous necrosis and thus a larger fraction of *Mtb* are present in a non-replicating state (Fig. 4E). Taken together, our model predicts that small reductions in IL-10 production rates can lead to increased frequency of sterile lesions; however, the remaining lesions are more difficult to sterilize (and most likely treat with antibiotics) as the bacterial populations shift to mainly non-replicating states.

Prediction 5: Activated Macrophage Derived IL-10 is Necessary to Control Antimicrobial Activity and Caseation in Simulated Granulomas

To determine whether a specific cellular source of IL-10 is most responsible for controlling antimicrobial activity and tissue caseation, we performed individual virtual deletions for each cellular source of IL-10 (activated macrophages, infected macrophages, and regulatory T cells). Deletion of activated-macrophage derived IL-10 causes the most significant change to bacterial loads, decreasing the mean CFU per lesion to ~50 CFU and increasing the number of sterile lesions ~8-fold (Fig. 5A). This is accompanied by a ~9-fold reduction in mean CFU/CEQ at day 50, indicating control over early antimicrobial activity (Fig. 5B). TNF is significantly elevated only at day 50 in both non-sterile and sterile lesions (Fig. 5C). In non-sterile lesions, caseous necrosis is increased ~1.4-fold at day 50, while sterile lesions show a ~1.6-fold increase in caseous necrosis at day 50 (Fig. 5D). Deletion of infected macrophage derived IL-10 leads to only a small decrease in CFU per lesion and a small increase in number of sterile lesions (Fig. 5A). Similarly, the mean CFU/CEQ is only reduced by ~1.2-fold at day 100 (Fig. 5B). TNF and caseous necrosis levels are not significantly different in both non-sterile and sterile lesions (Fig. 5D). Finally, deletion of regulatory T-cell derived IL-10 does not significantly change the mean CFU per lesion, average TNF levels, and caseous necrosis levels, but marginally increases the mean CFU/CEQ at day 50 (Fig. 5). These results suggest that activated macrophage production of IL-10 is primarily responsible for effectively controlling the antimicrobial activity of the immune response to infection while limiting the amount of host-induced caseation (Supplemental Fig. S2).

Prediction 6: Increased Infected Macrophage Derived IL-10 Can Shift Control of the Early Immune Response from Host to Pathogen

Some strains of *Mtb* can induce greater production of IL-10 from macrophages, which may have evolved as an efficient strategy to limit bacterial sterilization (1). Furthermore, neutrophils may play a key role in dictating increased levels of IL-10 production from infected macrophages (25–27). Although infected macrophage IL-10 production appears to have limited control over antimicrobial activity, production rates of IL-10 from both activated and infected macrophages are positively correlated with CFU per lesion and CFU/CEQ at day 50 and 200 (see sensitivity analysis in Supplemental Table II). Therefore, we tested how increased production of IL-10 from infected macrophages might undermine host control of antimicrobial activity and promote pathogen persistence.

As the fractional synthesis rate of IL-10 from infected macrophages (Eqn. 2) is increased, there is a linear increase in the percentage of IL-10 in the lesion that is derived from infected macrophages (Pearson's r = 0.9265, p < 0.0001) (Fig. 6A). In contrast, CFU per lesion, CFU/CEQ, and macrophage populations respond to increased IL-10 synthesis by infected macrophages in a highly non-linear fashion. We predict multiple regimes of IL-10 control over antimicrobial activity labeled as Regions 1–3 (Fig. 6B–D). In *Region 1* (low IL-10 synthesis rate), there is host-control where activated macrophages are the dominant population producing IL-10 leading to an efficient antimicrobial response and control of CFU per lesion. In *Region 2* (intermediate IL-10 synthesis rate), there is a transitional response wherein activated macrophages are the dominant population producing IL-10, but

production of IL-10 from infected macrophages is decreasing antimicrobial activity, causing a rise in CFU per lesion. In *Region 3* (high IL-10 synthesis rate), there is pathogen-control where infected macrophages (which are much less efficient killers than activated macrophages) are the dominant cell type producing IL-10 and antimicrobial activity is reduced ~10-fold at day 50 and 0 to 10-fold at day 200 (Fig. 6C). Reduction of antimicrobial activity causes the mean CFU per lesion at day 200 to increase ~100-fold (from lesions classified as *controlled growth* to *uncontrolled growth*) and the dominant macrophage population to switch from activated macrophages to infected macrophages (Fig. 6B, 6D). The large increase in CFU per lesion at high IL-10 levels may reflect a transition towards an outcome similar to TB pneumonia, where limited antimicrobial activity leads to uncontrolled bacterial replication that causes excessive inflammation and accompanying gross pathology (52). Together, these findings suggest that increased infected macrophage production rates of IL-10 can be an effective bacterial immune-evasion strategy that shifts control of antimicrobial activity from the host-immune response to the pathogen-derived response, therefore promoting pathogen persistence and survival.

Discussion

Many pro and anti-inflammatory mediators are involved in the host response to *Mtb* infection in the lung. Dissecting the individual roles of each cytokine in an *in vivo* setting that is similar to humans has been difficult. Here, we modify our established computational model (*GranSim*) to probe the role of the anti-inflammatory cytokine IL-10 during the immune response to *Mtb* over time and at an individual granuloma scale. Particular strengths of our computational approach include: using a model that has been calibrated and validated against temporal bacterial dynamics in the NHP model of TB, the ability to track the evolution of and retain the history of individual lesions, and the ability to modulate IL-10 production in granulomas as both a function of time and from particular cell subpopulations. These types of experiments would be difficult or impossible to perform in NHP or other experimental models of infection but are necessary to determining IL-10 mechanisms in TB. Understanding the complex host-pathogen interactions and immune responses controlled by IL-10 will aid in the development of new therapeutics for TB.

We calibrated and validated our established computational model of *Mtb* infection with bacterial dynamic data derived from the NHP model. Peak bacterial loads occur approximately 28 days post-infection and are followed by a sudden drop due to the onset of host adaptive immunity (Fig. 7A). Our model predicts a number of mechanistic roles for IL-10 including: (1) decreased levels of IL-10 lead to increased numbers of sterile lesions, but at the cost of early increased host caseation (Fig. 7), (2) small increases in early antimicrobial activity cause increased lesion sterility, (3) IL-10 produced by activated macrophages is a major mediator of early antimicrobial activity and early host-induced caseation and (4) increasing levels of infected macrophage derived IL-10 promotes bacterial persistence by limiting the early antimicrobial response and preventing lesion sterilization. It is likely that these predicted effects would not be observed in a murine model of *Mtb* infection as bacterial dynamics are significantly different (progressive infection) than those in NHPs and humans of which our computational model is based upon (65).

In humans, IL-10 levels are elevated in the lungs, bronchoalveolar lavage fluid, sputum, and serum of patients with active TB (1, 67, 68). Additionally, polymorphisms in IL-10 associated genes have been linked to increased susceptibility to TB (1). In mice, overexpression of IL-10 in macrophages or in entire animals is associated with higher bacterial loads in granulomas (47, 48). Recently, investigations in NHP models of TB suggest similar antimicrobial activity in lesions of both the active and latent disease state. The only significant difference between lesions in differing disease states was a substantially increased fraction of sterile lesions per animal in the latent state (52). Our model predicts that IL-10 contributes to sterilization on an individual granuloma basis, which suggests that IL-10 (and more generally anti-inflammatory mediators) could be a key regulator between the clinical outcomes of latent versus active disease by controlling lesional sterility.

Although IL-10 helps control bacterial load after the onset of the host-immune response, an inherent carrying capacity may exist in forming granulomas (52). Indeed the maximal observed CFU in a NHP model of infection is ~10^5 per lesion, comparing well with our calculations that suggest lesions without host-immunity have a maximal CFU of ~10^4-10^6 per lesion. If antimicrobial activity is not sufficient to sterilize a lesion, the level of IL-10 controls a bacterial set-point of the lesion, which is the balance between bacterial replication and antimicrobial response, with the benefit of reduced tissue caseation than sterilized lesions (Fig. 7). The idea of a set-point stems from studies on HIV-1 infection; post peak viremia, after host immunity is initiated, the virus is suppressed to a specific level (i.e. the set-point) that determines long-term progression to disease (69, 70). We predict that IL-10 transiently influences antimicrobial activity, controls granuloma outcome (sterile vs. non-sterile lesions), determines bacterial set-point, and limits the extent of host-induced tissue caseation at the lesional scale.

It has long been thought that IL-10 may play a central role in preventing an over-exuberant immune response during *Mtb* infection that leads to tissue damage (1, 7, 10, 28, 71, 72). Data from murine models are surprisingly limited, with only a single report of IL-10 K/O mice demonstrating increased pulmonary inflammation causing animals to succumb to infection earlier than WT mice (28). Using our *in silico* model we predict that IL-10 controls host-immunity induced caseation, especially during the initial burst of antimicrobial processes after the onset of adaptive immunity (30–60 days post-infection). Furthermore, we predict that increases in lesional sterility, due to increased antimicrobial effects, are at the expense of early increased host-induced caseous necrosis (Fig. 7). This is in agreement with our previous study, which predicted that the ratio of TNF and IL-10 is a critical mediator of infection control with limited host-induced damage (8). Our predictions agree well with the balance of damage and host response seen in many forms of disease pathogenesis (40).

Although we approximated tissue damage by measuring levels of caseous necrosis, it is important to note that tissue damage *in vivo* is a much more complicated process attributed to a myriad of host processes. We are currently evaluating better measurements of tissue damage (e.g. differentiating between apoptosis and necrosis, as well as fibrosis) and immunopathology (e.g. neutrophils) that could be added to our model. Because *Mtb* infection can lead to chronic cell death and high levels of caseous necrosis, we anticipate that better measurements of tissue damage could point to an even clearer role for IL-10 and

help define the mechanisms preventing host-immunity induced tissue damage. In addition, our model includes only a simple description of hypoxia, wherein bacteria transition to a slowly replicating state in compartments labeled as caseous necrosis. Although this model is able to qualitatively replicate a caseous necrotic region in the center of lesions where bacteria do not grow, the direct impact of reduced pH and available oxygen on the effects of cytokines and bacteria growth are not directly considered. However, due to the location of the caseous necrosis at the center of the lesion and the restricted movement of cells (both *in vivo* and *in silico*) into caseous necrotic compartments, viable immune cells rarely accumulate in this region and therefore the effects of decreased oxygen tension and pH on the effects of cytokines and cell viability are likely to be minimal. We are currently developing a detailed mechanistic description of *Mtb* growth in response to environmental cues such as oxygen and nutrients, which will allow for further characterization of *Mtb* dynamics in caseous necrotic regions.

IL-10 is not the only regulatory and anti-inflammatory cytokine present during infection. It has been suggested in murine models that a lack of data indicating a role for IL-10 in preventing tissue damage may be due the role of other regulatory mechanisms (such as PD-1 bearing T cells or TGF-β) (7, 28, 73, 74). Our model indicates that in the absence of IL-10, increased caseous necrosis at later stages post-infection (150–300 days) can be partially controlled by other regulatory mechanisms included in the model, such as cell-cell contact mediated down-regulation by T cells and tissue remodeling (data not shown). Additionally, human and macaque lesions can resolve by fibrotic processes that are likely driven by TGF-β (3). We are currently working on integrating fibrotic pathways into our model to understand the basis of fibrosis during TB. This should lead to a deeper understanding of how IL-10-based control of early tissue damage may be important in preventing later development of fibrosis and scarring in lesions.

The major source of IL-10 identified by our studies is activated macrophages. Although regulatory T cells produce IL-10 at twice the rate of activated macrophages in our model, there are a limited number of regulatory T cells recruited to the lesion and their localization in the periphery restricts effectiveness of their specific IL-10 production. IL-10 production may not only be a host-derived protective mechanism, but a pathogen-evolved bactericidal evasion mechanism. In many chronic infection scenarios (both viral and bacterial) pathogenic IL-10 induction can be used to dull the efficacy of the immune response (1, 7, 75). Specifically, in TB infection the *Mtb* clinical strains HN878 and CH have been shown to induce increased levels of IL-10 production from infected macrophages that could help establish a state of chronic infection (1, 11–16). Additionally, increased IL-10 levels in human patients are correlated with poor outcomes of TB infection (67, 68, 76, 77). Using our computational model we predicted that high levels of IL-10 derived from infected macrophages promotes pathogen persistence by limiting antimicrobial activity of the early immune response to *Mtb*. Reduction of antimicrobial activity increases the chances that a healthy macrophage will engulf *Mtb* (promoting pathogen persistence), while allowing the pathogen to survive in its intracellular niche by preventing cellular apoptosis/necrosis (75). These mechanisms prevent lesions from sterilizing and increase the bacterial set-point at the late stages of infection (Fig. 7A). Furthermore, we show that a switch in lesional control

occurs at high levels of IL-10 derived from infected macrophages (Fig. 6) where the ability of activated macrophages to use IL-10 as a regulatory mechanism for host protection (prevention of host-induced caseation) is lost and the pathogen is able to repurpose IL-10 as a mechanism of persistence ('immune-evasion').

A limitation of the current study is that neutrophils are not included in this model, as their contributions to pathology or protection are not clearly understood (78). Neutrophils are present in TB granulomas, however in the vast majority of lesions neutrophil populations are lower than both T cells and macrophages (1, 78). Neutrophils can produce IL-10 in response to mycobacterial stimulation and neutrophil infiltration has been associated with poor TB outcomes (25, 26, 79) (J. Mattila, J. Flynn – unpublished data). Although neutrophils are different cells with a distinct gene and protease expression profile than macrophages, from a modeling perspective where these differences in genes and proteases are not considered, neutrophils would function in a manner similar to macrophages: engaging in phagocytic activities, providing an intracellular niche for *Mtb* growth, and producing IL-10 upon appropriate stimulation (26, 27, 80–82). Based on our prediction that increased IL-10 production from infected macrophages limits the early antimicrobial immune response, parallels could be considered for neutrophil IL-10 production. Therefore, many questions could be addressed by a future version of our model that incorporates an accurate description of neutrophils: How do neutrophils contribute to caseous necrosis? What stimuli induce neutrophil IL-10 expression? Does IL-10 production by neutrophils limit or promote caseous necrosis? Although neutrophils and neutrophil-related processes have been clinically correlated with poor TB outcomes, much of the existing data on neutrophil behavior (e.g. cytokine production rates, phagocytotic rates, free radical production rates) come from murine models of TB, which may not be reflective of what occurs in humans and NHPs. Our group is currently gathering experimental data regarding neutrophils in the NHP model of TB in order to accurately describe neutrophils in a next-generation computational model.

Our computational platform has allowed us to understand the role of IL-10 in controlling the trade-off between antimicrobial activity of the early immune response to *Mtb*, lesional sterility, and host-immunity derived tissue caseation. Our unique multi-scale computational platform used in parallel with experimental models provides an integrated systems biology approach to better understand the complex immune response to *Mtb*, which will allow us to rapidly hypothesize and test novel therapeutic interventions. For instance, our simulations of IL-10 depletion or decreased rates of IL-10 secretion suggest that novel IL-10 focused treatment strategies (e.g. anti-IL10R antibodies) may be effective if properly timed during the adaptive immune response to promote lesional sterility. Furthermore, modulating IL-10 levels in the context of other important immune molecules (e.g. TNF or IFN-γ) could prove to be beneficial in controlling lesion outcome, but have yet to be explored (83–85). Unfortunately, these strategies may lack clinical relevance in humans because the short window where IL-10 treatments could be effective is at odds with the long-time-to-diagnosis in clinics. Thus, our predictions further underscore the importance of early events in infection and the need for developing novel diagnostics to facilitate early diagnosis and intervention in *Mtb* infection.

Supplementary Material

Refer to Web version on PubMed Central for supplementary material.

Acknowledgements

References

1. O'Garra A, Redford PS, McNab FW, Bloom CI, Wilkinson RJ, Berry MPR. The immune response in tuberculosis. Annu. Rev. Immunol. 2013; 31:475–527. [PubMed: 23516984]

2. Ouyang W, Rutz S, Crellin NK, a Valdez P, Hymowitz SG. Regulation and functions of the IL-10 family of cytokines in inflammation and disease. Annu. Rev. Immunol. 2011; 29:71–109. [PubMed: 21166540]

3. Flynn JL, Chan J. Immunology of tuberculosis. Annu. Rev. Immunol. 2001; 19:93–129. [PubMed: 11244032]

4. Moore KW, de Waal Malefyt R, Coffman RL, O'Garra A. Interleukin-10 and the interleukin-10 receptor. Annu. Rev. Immunol. 2001; 19:683–765. [PubMed: 11244051]

5. Bogdan C. Macrophage deactivation by interleukin 10. J. Exp. Med. 1991; 174:1549–1555. [PubMed: 1744584]

6. Balcewicz-Sablinska MK, Gan H, Remold HG. Interleukin 10 produced by macrophages inoculated with Mycobacterium avium attenuates mycobacteria-induced apoptosis by reduction of TNF-alpha activity. J. Infect. Dis. 1999; 180:1230–1237. [PubMed: 10479152]

7. Redford PS, Murray PJ, O'Garra A. The role of IL-10 in immune regulation during M. tuberculosis infection. Mucosal Immunol. 2011; 4:261–270. [PubMed: 21451501]

8. Cilfone NA, Perry CR, Kirschner DE, Linderman JJ. Multi-scale modeling predicts a balance of tumor necrosis factor-α and interleukin-10 controls the granuloma environment during Mycobacterium tuberculosis infection. PLoS One. 2013; 8:e68680. [PubMed: 23869227]

9. Gordon S. Alternative activation of macrophages. Nat. Rev. Immunol. 2003; 3:23–35. [PubMed: 12511873]

10. Wigginton JE, Kirschner D. A model to predict cell-mediated immune regulatory mechanisms during human infection with Mycobacterium tuberculosis. J. Immunol. 2001; 166:1951–1967. [PubMed: 11160244]

11. Manca C, Tsenova L, Barry CE, Bergtold A, Freeman S, a Haslett P, Musser JM, Freedman VH, Kaplan G. Mycobacterium tuberculosis CDC1551 induces a more vigorous host response in vivo and in vitro, but is not more virulent than other clinical isolates. J. Immunol. 1999; 162:6740–6746. [PubMed: 10352293]

12. Ordway D, Henao-Tamayo M, Harton M, Palanisamy G, Troudt J, Shanley C, Basaraba RJ, Orme IM. The hypervirulent Mycobacterium tuberculosis strain HN878 induces a potent TH1 response followed by rapid down-regulation. J. Immunol. 2007; 179:522–531. [PubMed: 17579073]

13. Portevin D, Gagneux S, Comas I, Young D. Human macrophage responses to clinical isolates from the Mycobacterium tuberculosis complex discriminate between ancient and modern lineages. PLoS Pathog. 2011; 7:e1001307. [PubMed: 21408618]

14. Newton SM, Smith RJ, Wilkinson KA, Nicol MP, Garton NJ, Staples KJ, Stewart GR, Wain JR, Martineau AR, Fandrich S, Smallie T, Foxwell B, Al-Obaidi A, Shafi J, Rajakumar K, Kampmann B, Andrew PW, Ziegler-Heitbrock L, Barer MR, Wilkinson RJ. A deletion defining a common Asian lineage of Mycobacterium tuberculosis associates with immune subversion. Proc. Natl. Acad. Sci. U. S. A. 2006; 103:15594–15598. [PubMed: 17028173]

15. Nair S, a Ramaswamy P, Ghosh S, Joshi DC, Pathak N, Siddiqui I, Sharma P, Hasnain SE, Mande SC, Mukhopadhyay S. The PPE18 of Mycobacterium tuberculosis interacts with TLR2 and activates IL-10 induction in macrophage. J. Immunol. 2009; 183:6269–6281. [PubMed: 19880448]

16. Cyktor JC, Turner J. Interleukin-10 and immunity against prokaryotic and eukaryotic intracellular pathogens. Infect. Immun. 2011; 79:2964–2973. [PubMed: 21576331]

17. O'Garra A, Vieira PL, Vieira P, Goldfeld AE. IL-10-producing and naturally occurring CD4+ Tregs: limiting collateral damage. J. Clin. Invest. 2004; 114:1372–1378. [PubMed: 15545984]

18. Yssel H, De Waal Malefyt R, Roncarolo MG, Abrams JS, Lahesmaa R, Spits H, de Vries JE. IL-10 is produced by subsets of human CD4+ T cell clones and peripheral blood T cells. J. Immunol. 1992; 149:2378–2384. [PubMed: 1356125]

19. Madura Larsen J, Benn CS, Fillie Y, van der Kleij D, Aaby P, Yazdanbakhsh M. BCG stimulated dendritic cells induce an interleukin-10 producing T-cell population with no T helper 1 or T helper 2 bias in vitro. Immunology. 2007; 121:276–282. [PubMed: 17371543]

20. Scott-Browne JP, Shafiani S, Tucker-Heard G, Ishida-Tsubota K, Fontenot JD, Rudensky AY, Bevan MJ, Urdahl KB. Expansion and function of Foxp3-expressing T regulatory cells during tuberculosis. J. Exp. Med. 2007; 204:2159–2169. [PubMed: 17709423]

21. Roncarolo MG, Gregori S, Battaglia M, Bacchetta R, Fleischhauer K, Levings MK. Interleukin-10-secreting type 1 regulatory T cells in rodents and humans. Immunol. Rev. 2006; 212:28–50. [PubMed: 16903904]

22. Ribeiro-Rodrigues R, Resende Co T, Rojas R, Toossi Z, Dietze R, Boom WH, Maciel E, Hirsch CS. A role for CD4+CD25+ T cells in regulation of the immune response during human tuberculosis. Clin. Exp. Immunol. 2006; 144:25–34. [PubMed: 16542361]

23. Gerosa F, Nisii C, Righetti S, Micciolo R, Marchesini M, Cazzadori A, Trinchieri G. CD4(+) T cell clones producing both interferon-gamma and interleukin-10 predominate in bronchoalveolar lavages of active pulmonary tuberculosis patients. Clin. Immunol. 1999; 92:224–234. [PubMed: 10479527]

24. Trinchieri G. Regulatory Role of T Cells Producing both Interferon gamma and Interleukin 10 in Persistent Infection. J. Exp. Med. 2001; 194:F53–F57. [PubMed: 11714761]

25. Braian C, Hogea V, Stendahl O. Mycobacterium tuberculosis- induced neutrophil extracellular traps activate human macrophages. J. Innate Immun. 2013; 5:591–602. [PubMed: 23635526]

26. Doz E, Lombard R, Carreras F, Buzoni-Gatel D, Winter N. Mycobacteria-infected dendritic cells attract neutrophils that produce IL-10 and specifically shut down Th17 CD4 T cells through their IL-10 receptor. J. Immunol. 2013; 191:3818–3826. [PubMed: 23997221]

27. Marzo E, Vilaplana C, Tapia G, Diaz J, Garcia V, Cardona P-J. Damaging role of neutrophilic infiltration in a mouse model of progressive tuberculosis. Tuberculosis (Edinb). 2014; 94:55–64. [PubMed: 24291066]

28. Higgins DM, Sanchez-Campillo J, Rosas-Taraco AG, Lee EJ, Orme IM, Gonzalez-Juarrero M. Lack of IL-10 alters inflammatory and immune responses during pulmonary Mycobacterium tuberculosis infection. Tuberculosis (Edinb). 2009; 89:149–157. [PubMed: 19213603]

29. Saunders BM, Britton WJ. Life and death in the granuloma: immunopathology of tuberculosis. Immunol. Cell Biol. 2007; 85:103–111. [PubMed: 17213830]

30. Via LE, Lin PL, Ray SM, Carrillo J, Allen SS, Eum SY, Taylor K, Klein E, Manjunatha U, Gonzales J, Lee EG, Park SK, a Raleigh J, Cho SN, McMurray DN, Flynn JL, Barry CE. Tuberculous granulomas are hypoxic in guinea pigs, rabbits, and nonhuman primates. Infect. Immun. 2008; 76:2333–2340. [PubMed: 18347040]

31. Kaufmann HSE, Dorhoi A. Inflammation in tuberculosis: interactions, imbalances and interventions. Curr. Opin. Immunol. 2013; 25:441–449. [PubMed: 23725875]

32. Wang L, Du F, Wang X. TNF-alpha induces two distinct caspase-8 activation pathways. Cell. 2008; 133:693–703. [PubMed: 18485876]

33. Fink SL, Cookson BT. Apoptosis, pyroptosis, and necrosis: mechanistic description of dead and dying eukaryotic cells. Infect. Immun. 2005; 73:1907–1916. [PubMed: 15784530]

34. Fayyazi, a; Eichmeyer, B.; Soruri, A.; Schweyer, S.; Herms, J.; Schwarz, P.; Radzun, HJ. Apoptosis of macrophages and T cells in tuberculosis associated caseous necrosis. J. Pathol. 2000; 191:417–425. [PubMed: 10918217]

35. Arcila ML, Sánchez MD, Ortiz B, Barrera LF, García LF, Rojas M. Activation of apoptosis, but not necrosis, during Mycobacterium tuberculosis infection correlated with decreased bacterial growth: role of TNF-alpha, IL-10, caspases and phospholipase A2. Cell. Immunol. 2007; 249:80–93. [PubMed: 18160064]

36. Rojas M, Olivier M, Gros P, Barrera LF, García LF. TNF-alpha and IL-10 modulate the induction of apoptosis by virulent Mycobacterium tuberculosis in murine macrophages. J. Immunol. 1999; 162:6122–6131. [PubMed: 10229855]

37. Keane J, Remold HG, Kornfeld H. Virulent Mycobacterium tuberculosis strains evade apoptosis of infected alveolar macrophages. J. Immunol. 2000; 164:2016–2020. [PubMed: 10657653]

38. Majno G, Joris I. Apoptosis, oncosis, and necrosis. An overview of cell death. Am. J. Pathol. 1995; 146:3–15. [PubMed: 7856735]

39. Laskin DL, Pendino KJ. Macrophages and inflammatory mediators in tissue injury. Annu. Rev. Pharmacol. Toxicol. 1995; 35:655–677. [PubMed: 7598511]

40. Casadevall A, Pirofski L. The damage-response framework of microbial pathogenesis. Nat. Rev. Microbiol. 2003; 1:17–24. [PubMed: 15040176]

41. Arcila ML, Sánchez MD, Ortiz B, Barrera LF, García LF, Rojas M. Activation of apoptosis, but not necrosis, during Mycobacterium tuberculosis infection correlated with decreased bacterial growth: role of TNF-alpha, IL-10, caspases and phospholipase A2. Cell. Immunol. 2007; 249:80–93. [PubMed: 18160064]

42. Zhang D-W, Shao J, Lin J, Zhang N, Lu B-J, Lin S-C, Dong M-Q, Han J. RIP3, an energy metabolism regulator that switches TNF-induced cell death from apoptosis to necrosis. Science. 2009; 325:332–336. [PubMed: 19498109]

43. He S, Wang L, Miao L, Wang T, Du F, Zhao L, Wang X. Receptor interacting protein kinase-3 determines cellular necrotic response to TNF-alpha. Cell. 2009; 137:1100–1111. [PubMed: 19524512]

44. Roca FJ, Ramakrishnan L. TNF dually mediates resistance and susceptibility to mycobacteria via mitochondrial reactive oxygen species. Cell. 2013; 153:521–534. [PubMed: 23582643]

45. Cyktor JC, Carruthers B, a Kominsky R, Beamer GL, Stromberg P, Turner J. IL-10 inhibits mature fibrotic granuloma formation during Mycobacterium tuberculosis infection. J. Immunol. 2013; 190:2778–2790. [PubMed: 23396944]

46. Pitt JM, Stavropoulos E, Redford PS, Beebe AM, Bancroft GJ, Young DB, O'Garra A. Blockade of IL-10 signaling during bacillus Calmette-Guérin vaccination enhances and sustains Th1, Th17, and innate lymphoid IFN-γ and IL-17 responses and increases protection to Mycobacterium tuberculosis infection. J. Immunol. 2012; 189:4079–4087. [PubMed: 22972927]

47. Lang R, Rutschman RL, Greaves DR, Murray PJ. Autocrine deactivation of macrophages in transgenic mice constitutively overexpressing IL-10 under control of the human CD68 promoter. J. Immunol. 2002; 168:3402–3411. [PubMed: 11907098]

48. Turner J, Gonzalez-Juarrero M, Ellis DL, Basaraba RJ, Kipnis A, Orme IM, Cooper AM. In vivo IL-10 production reactivates chronic pulmonary tuberculosis in C57BL/6 mice. J. Immunol. 2002; 169:6343–6351. [PubMed: 12444141]

49. Shaler CR, Horvath CN, Jeyanathan M, Xing Z. Within the Enemy's Camp: contribution of the granuloma to the dissemination, persistence and transmission of Mycobacterium tuberculosis. Front. Immunol. 2013; 4:30. [PubMed: 23420646]

50. Modlin RL, Bloom BR. TB or not TB: that is no longer the question. Sci. Transl. Med. 2013; 5 213sr6.

51. Seok J, Warren HS, Cuenca AG, Mindrinos MN, V Baker H, Xu W, Richards DR, McDonald-Smith GP, Gao H, Hennessy L, Finnerty CC, López CM, Honari S, Moore EE, Minei JP, Cuschieri J, Bankey PE, Johnson JL, Sperry J, Nathens AB, Billiar TR, a West M, Jeschke MG, Klein MB, Gamelli RL, Gibran NS, Brownstein BH, Miller-Graziano C, Calvano SE, Mason PH, Cobb JP, Rahme LG, Lowry SF, V Maier R, Moldawer LL, Herndon DN, Davis RW, Xiao W, Tompkins RG. Genomic responses in mouse models poorly mimic human inflammatory diseases. Proc. Natl. Acad. Sci. U. S. A. 2013; 110:3507–3512. [PubMed: 23401516]

52. Lin PL, Ford CB, Coleman MT, Myers AJ, Gawande R, Ioerger T, Sacchettini J, Fortune SM, Flynn JL. Sterilization of granulomas is common in active and latent tuberculosis despite within-host variability in bacterial killing. Nat. Med. 2014; 20:75–79. [PubMed: 24336248]

53. Ray CJJ, Flynn JL, Kirschner DE. Synergy between individual TNF-dependent functions determines granuloma performance for controlling Mycobacterium tuberculosis infection. J. Immunol. 2009; 182:3706–3717. [PubMed: 19265149]

54. Fallahi-Sichani M, El-Kebir M, Marino S, Kirschner DE, Linderman JJ. Multiscale computational modeling reveals a critical role for TNF-α receptor 1 dynamics in tuberculosis granuloma formation. J. Immunol. 2011; 186:3472–3483. [PubMed: 21321109]

55. Lin PL, Rodgers M, Smith L, Bigbee M, Myers A, Bigbee C, Chiosea I, V Capuano S, Fuhrman C, Klein E, Flynn JL. Quantitative comparison of active and latent tuberculosis in the cynomolgus macaque model. Infect. Immun. 2009; 77:4631–4642. [PubMed: 19620341]

56. Lin PL, Dartois V, Johnston PJ, Janssen C, Via L, Goodwin MB, Klein E, Barry CE, Flynn JL. Metronidazole prevents reactivation of latent Mycobacterium tuberculosis infection in macaques. Proc. Natl. Acad. Sci. U. S. A. 2012; 109:14188–14193. [PubMed: 22826237]

57. Lin PL, Coleman T, Carney JPJ, Lopresti BJ, Tomko J, Fillmore D, Dartois V, Scanga C, Frye LJ, Janssen C, Klein E, Barry CE, Flynn JL. Radiologic responses in cynomolgous macaques for assessing tuberculosis chemotherapy regimens. Antimicrob. Agents Chemother. 2013; 57:4237–4244.

58. Lin PL, Myers A, Smith L, Bigbee C, Bigbee M, Fuhrman C, Grieser H, Chiosea I, Voitenek NN, V Capuano S, Klein E, Flynn JL. Tumor necrosis factor neutralization results in disseminated disease in acute and latent Mycobacterium tuberculosis infection with normal granuloma structure in a cynomolgus macaque model. Arthritis Rheum. 2010; 62:340–350. [PubMed: 20112395]

59. Flynn JL, Chan J, Triebold KJ, Dalton DK, a Stewart T, Bloom BR. An essential role for interferon gamma in resistance to Mycobacterium tuberculosis infection. J. Exp. Med. 1993; 178:2249–2254. [PubMed: 7504064]

60. Gideon HP, Flynn JL. Latent tuberculosis: what the host "sees"? Immunol. Res. 2011; 50:202–212. [PubMed: 21717066]

61. Lin PL, Flynn JL. Understanding latent tuberculosis: a moving target. J. Immunol. 2010; 185:15–22. [PubMed: 20562268]

62. Via LE, Weiner DM, Schimel D, Lin PL, Dayao E, Tankersley SL, Cai Y, Coleman MT, Tomko J, Paripati P, Orandle M, Kastenmayer RJ, Tartakovsky M, Rosenthal A, Portevin D, Eum SY, Lahouar S, Gagneux S, Young DB, Flynn JL, Barry CE. Differential Virulence and Disease Progression following Mycobacterium tuberculosis Complex Infection of the Common Marmoset (Callithrix jacchus). Infect. Immun. 2013; 81:2909–2919. [PubMed: 23716617]

63. Marino S, Hogue IB, Ray CJ, Kirschner DE. A methodology for performing global uncertainty and sensitivity analysis in systems biology. J. Theor. Biol. 2008; 254:178–196. [PubMed: 18572196]

64. Lin PL, Pawar S, Myers A, Pegu A, Fuhrman C, a Reinhart T, V Capuano S, Klein E, Flynn JL. Early events in Mycobacterium tuberculosis infection in cynomolgus macaques. Infect. Immun. 2006; 74:3790–3803. [PubMed: 16790751]

65. Flynn JL, Chan J. Immunology of tuberculosis. Annu. Rev. Immunol. 2001; 19:93–129. [PubMed: 11244032]

66. Bean AG, Roach DR, Briscoe H, France MP, Korner H, Sedgwick JD, Britton WJ. Structural deficiencies in granuloma formation in TNF gene-targeted mice underlie the heightened susceptibility to aerosol Mycobacterium tuberculosis infection, which is not compensated for by lymphotoxin. J. Immunol. 1999; 162:3504–3511. [PubMed: 10092807]

67. Verbon, a; Juffermans, N.; Van Deventer, SJ.; Speelman, P.; Van Deutekom, H.; Van Der Poll, T. Serum concentrations of cytokines in patients with active tuberculosis (TB) and after treatment. Clin. Exp. Immunol. 1999; 115:110–113. [PubMed: 9933428]

68. Bonecini-Almeida MG, Ho JL, Boechat N, Huard RC, Chitale S, Doo H, Geng J, Rego L, Lazzarini LCO, Kritski AL, Johnson WD, McCaffrey TA, e Silva JRL. Down-Modulation of Lung Immune Responses by Interleukin-10 and Transforming Growth Factor (TGF-) and Analysis of TGF- Receptors I and II in Active Tuberculosis. Infect. Immun. 2004; 72:2628–2634. [PubMed: 15102771]

69. Ho DD, Neumann AU, Perelson AS, Chen W, Leonard JM, Markowitz M. Rapid turnover of plasma virions and CD4 lymphocytes in HIV-1 infection. Nature. 1995; 373:123–126. [PubMed: 7816094]

70. Masel J, Arnaout RA, O'Brien TR, Goedert JJ, Lloyd AL. Fluctuations in HIV-1 viral load are correlated to CD4+ T-lymphocyte count during the natural course of infection. J. Acquir. Immune Defic. Syndr. 2000; 23:375–379. [PubMed: 10866229]

71. Lin C-L, Tawhai MH, Hoffman Ea. Multiscale image-based modeling and simulation of gas flow and particle transport in the human lungs. Wiley Interdiscip. Rev. Syst. Biol. Med. 2013; 5:643–655. [PubMed: 23843310]

72. Flynn JL, Chan J, Lin PL. Macrophages and control of granulomatous inflammation in tuberculosis. Mucosal Immunol. 2011; 4:271–278. [PubMed: 21430653]

73. Barber DL, Mayer-Barber KD, Feng CG, Sharpe AH, Sher A. CD4 T cells promote rather than control tuberculosis in the absence of PD-1-mediated inhibition. J. Immunol. 2011; 186:1598–1607. [PubMed: 21172867]

74. Lázár-Molnár E, Chen B, a Sweeney K, Wang EJ, Liu W, Lin J, a Porcelli S, Almo SC, Nathenson SG, Jacobs WR. Programmed death-1 (PD-1)-deficient mice are extraordinarily sensitive to tuberculosis. Proc. Natl. Acad. Sci. U. S. A. 2010; 107:13402–13407. [PubMed: 20624978]

75. Redpath S, Ghazal P, Gascoigne NR. Hijacking and exploitation of IL-10 by intracellular pathogens. Trends Microbiol. 2001; 9:86–92. [PubMed: 11173248]

76. Olobo JO, Geletu M, a Demissie, Eguale T, Hiwot K, Aderaye G, Britton S. Circulating TNF-alpha, TGF-beta, and IL-10 in tuberculosis patients and healthy contacts. Scand. J. Immunol. 2001; 53:85–91. [PubMed: 11169211]

77. Jamil B, Shahid F, Hasan Z, Nasir N, Razzaki T, Dawood G, Hussain R. Interferon gamma/IL10 ratio defines the disease severity in pulmonary and extra pulmonary tuberculosis. Tuberculosis (Edinb). 2007; 87:279–287. [PubMed: 17532265]

78. Lowe DM, Redford PS, Wilkinson RJ, O'Garra A, Martineau AR. Neutrophils in tuberculosis: friend or foe? Trends Immunol. 2012; 33:14–25. [PubMed: 22094048]

79. Cooper AM, Torrado E. Protection versus pathology in tuberculosis: recent insights. Curr. Opin. Immunol. 2012; 24:431–437. [PubMed: 22613092]

80. Blomgran R, Desvignes L, Briken V, Ernst JD. Mycobacterium tuberculosis inhibits neutrophil apoptosis, leading to delayed activation of naive CD4 T cells. Cell Host Microbe. 2012; 11:81–90. [PubMed: 22264515]

81. Eum S-Y, Kong J-H, Hong M-S, Lee Y-J, Kim J-H, Hwang S-H, Cho S-N, Via LE, Barry CE. Neutrophils are the predominant infected phagocytic cells in the airways of patients with active pulmonary TB. Chest. 2010; 137:122–128. [PubMed: 19749004]

82. Bru A, Cardona P-J. Mathematical modeling of tuberculosis bacillary counts and cellular populations in the organs of infected mice. PLoS One. 2010; 5:e12985. [PubMed: 20886087]

83. Debs RJ, Fuchs HJ, Philip R, Montgomery AB, Brunette EN, Liggitt D, Patton JS, Shellito JE. Lung-specific delivery of cytokines induces sustained pulmonary and systemic immunomodulation in rats. J. Immunol. 1988; 140:3482–3488. [PubMed: 3283235]

84. Huhn RD, Radwanski E, O'Connell SM, Sturgill MG, Clarke L, Cody RP, Affrime MB, Cutler DL. Pharmacokinetics and immunomodulatory properties of intravenously administered recombinant human interleukin-10 in healthy volunteers. Blood. 1996; 87:699–705. [PubMed: 8555493]

85. Kramp JC, McMurray DN, Formichella C, Jeevan A. The in vivo immunomodulatory effect of recombinant tumour necrosis factor-alpha in guinea pigs vaccinated with Mycobacterium bovis bacille Calmette-Guérin. Clin. Exp. Immunol. 2011; 165:110–120. [PubMed: 21545584]
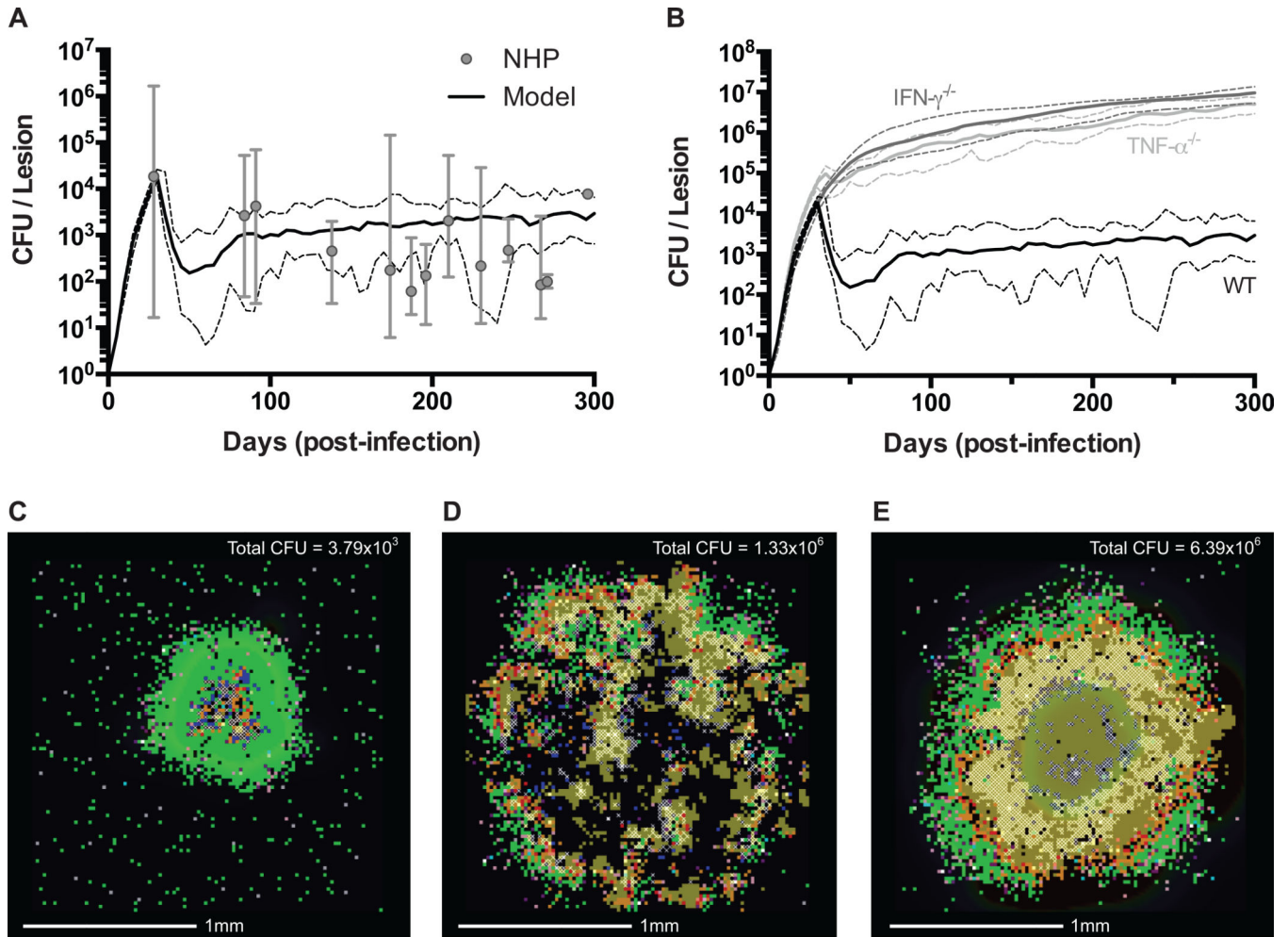
Figure 1. Model validation of simulated lesions
A. Comparison of scaled CFU per lesion between best-fit WT simulated lesions (N = 25) (52) (median – solid line, min/max – dashed lines) and NHP data collected between 28 and 296 days post-infection (N = 32) (median – filled circles, min/max – error bars). B. Comparison of scaled CFU per lesion for simulated lesions of TNF-α (median – light grey line, min/max – dashed light grey lines) and IFN-γ (median – dark grey line, min/max – dashed dark grey lines) deletions compared to WT simulated lesions (median – solid black line, min/max – dashed black lines) (N = 20). C. Snapshot of a WT lesion at 200 days post-infection. D. Snapshot of a TNF-α deletion lesion at 200 days post-infection. E. Snapshot of an IFN-γ deletion lesion at 200 days post-infection. Total scaled CFU for each lesion is indicated in the upper corner. Snapshot legend colors as follows: resting macrophages (green), infected macrophages (orange), chronically infected macrophage (red), activated macrophage (dark blue), pro-inflammatory T cell (pink), cytotoxic T cell (purple), regulatory T cell (aqua), extracellular bacteria (brown), and caseation (cross-hatch). These same colors are used for all subsequent images.
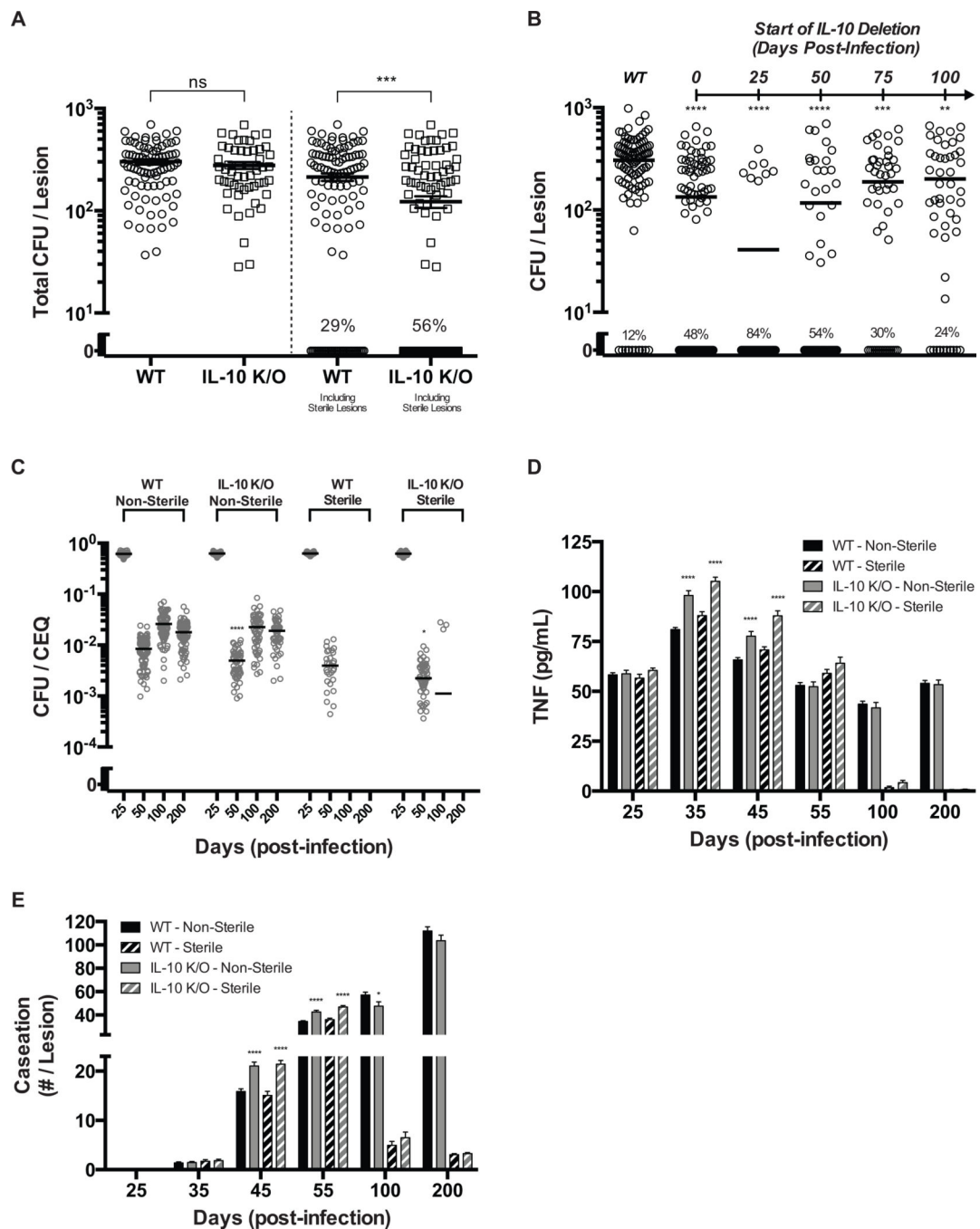
Figure 2. Virtual IL-10 deletions demonstrate control of the early immune response leads to increased sterilization of lesions

A. CFU for WT and IL-10 deletion (IL-10 K/O) lesions at 200 days post-infection. Individual circles and squares represent individual lesions. Lines indicate mean values. Percent of lesions becoming sterile by 200 days (out of 100 simulations) is indicated. B. CFU for WT and IL-10 deletions starting at days 25, 50, 75, and 100 post-infection (IL-10 K/O). Individual circles and squares represent individual lesions. Lines indicate mean values. Percent of lesions becoming sterile by 200 days (out of 100 simulations) is indicated. C. CFU/CEQ for outcome-specific WT and IL-10 K/O lesions. Outcomes are grouped as

non-sterile or sterile. Individual circles represent individual lesions. Lines indicate mean values. D–E. Average lesion TNF-α concentration and caseation for WT (black bars) and IL-10 K/O (grey bars) lesions. Caseation is measured by the number of grid sites affected. Non-sterile lesions are displayed as solid bars and sterile lesions are displayed as striped bars. Bars are representative of mean values with error bars showing SEM. For all panels, comparisons are made between the same granuloma classifications (e.g. non-sterile vs. non-sterile): * p 0.05, ** p 0.01, *** p 0.001, **** p 0.0001, N = 100 for A, C–E). N = 50 for B.
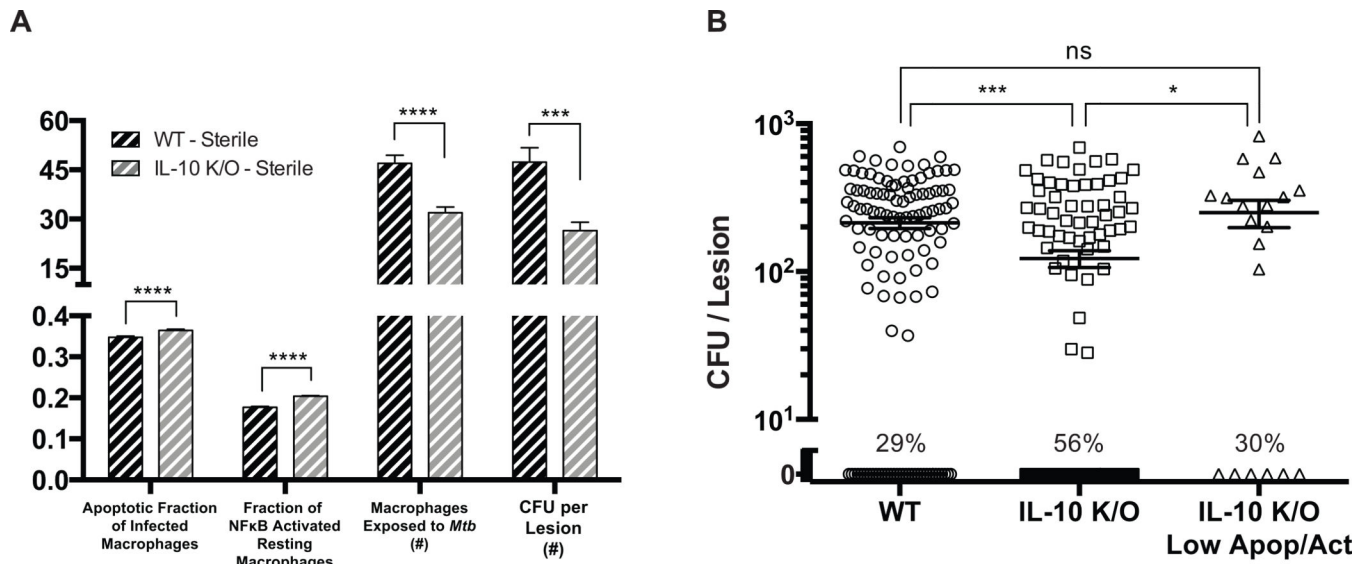
Figure 3. Comparison of simulated lesions that become sterile for WT and IL-10 deletions
A. Apoptotic fraction of infected macrophages, fraction of NFκB activated resting macrophages, number of macrophages exposed to *Mtb*, and CFU per lesion at 45 days post-infection for WT (black bars) and IL-10 K/O (grey bars) granulomas. B. CFU for WT, IL-10 K/O, and IL-10 K/O Low Apop/Act (decreased rates of apoptosis and NFκB activation) lesions at 200 days post-infection. Individual dots represent individual lesions. Lines indicate the mean values. Percentage of lesions becoming sterile by 200 days is indicated. Bars are representative of mean values with error bars showing SEM. For all panels: * p 0.05, ** p 0.01, *** p 0.001, **** p 0.0001, N = 100 for WT and IL-10 K/O simulations. N = 20 for IL-10 K/O Low Apop/Act simulations.
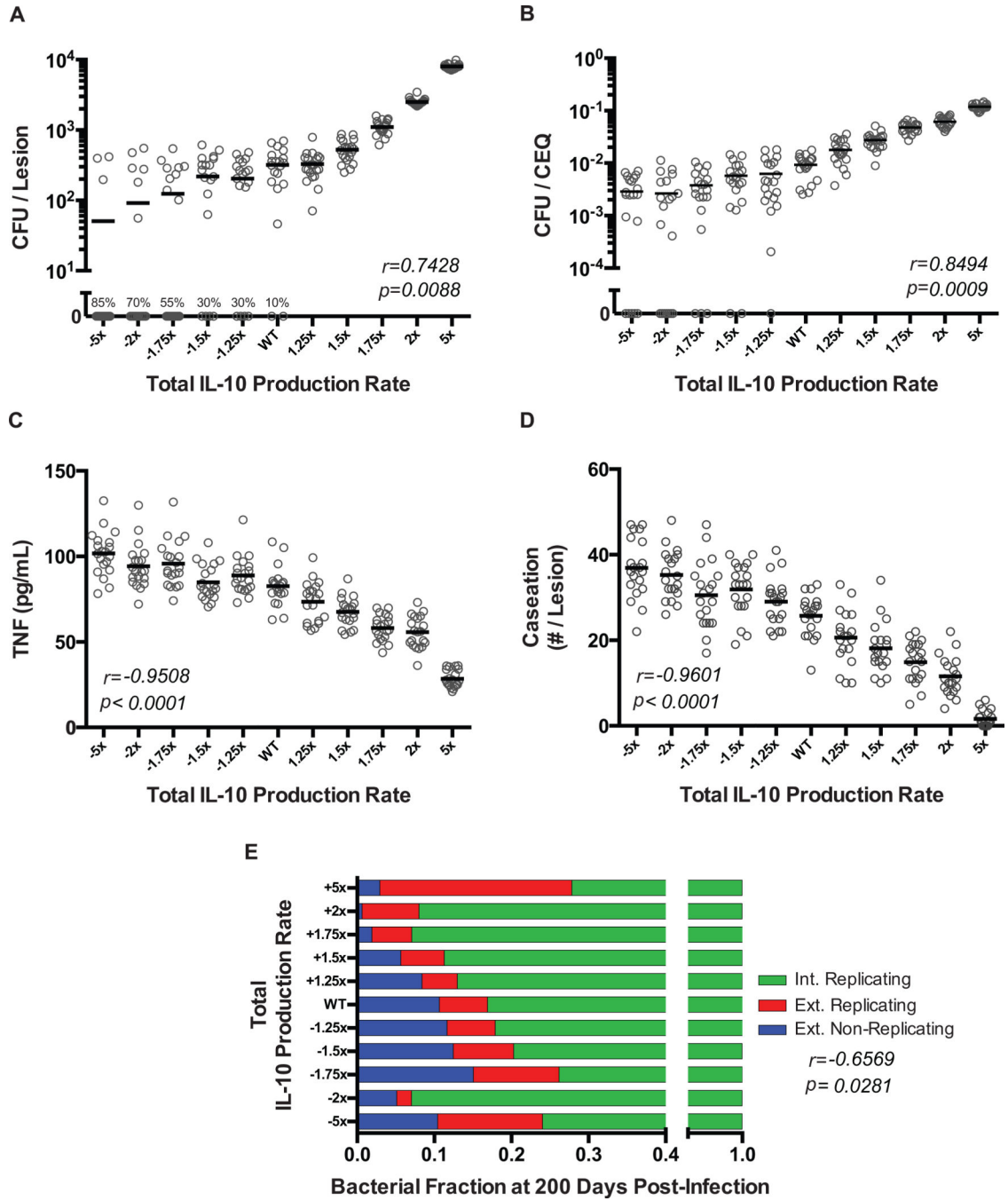
Figure 4. Simulations changing total levels of IL-10 production demonstrate control of bacterial set-point, outcome, and tissue damage

A. CFU comparisons for differing levels of total IL-10 production (5-fold reduction to 5-fold increase) at 200 days post-infection. The percentage indicates the number of sterile lesions at 200 days post-infection (chi-squared trend test, p<0.0001). B. CFU/CEQ comparisons for differing levels of total IL-10 production (5-fold reduction to 5-fold increase) at 200 days post-infection. C. Average lesion TNF-α concentration for differing levels of total IL-10 production (5-fold reduction to 5-fold increase) at 35 days post-infection. D. Average amounts of caseation for differing levels of total IL-10 production (5-

fold reduction to 5-fold increase) at 50 days post-infection. E. Fractions of bacterial populations in non-sterile lesions for differing levels of total IL-10 production (5-fold reduction shown by a minus sign to 5-fold increase) at 200 days post-infection. Individual dots represent individual lesions. Lines indicate the mean values. For all panels: Pearson correlation coefficients (*r*) and p-values (*p*) were calculated to determine the significance of observed trends.
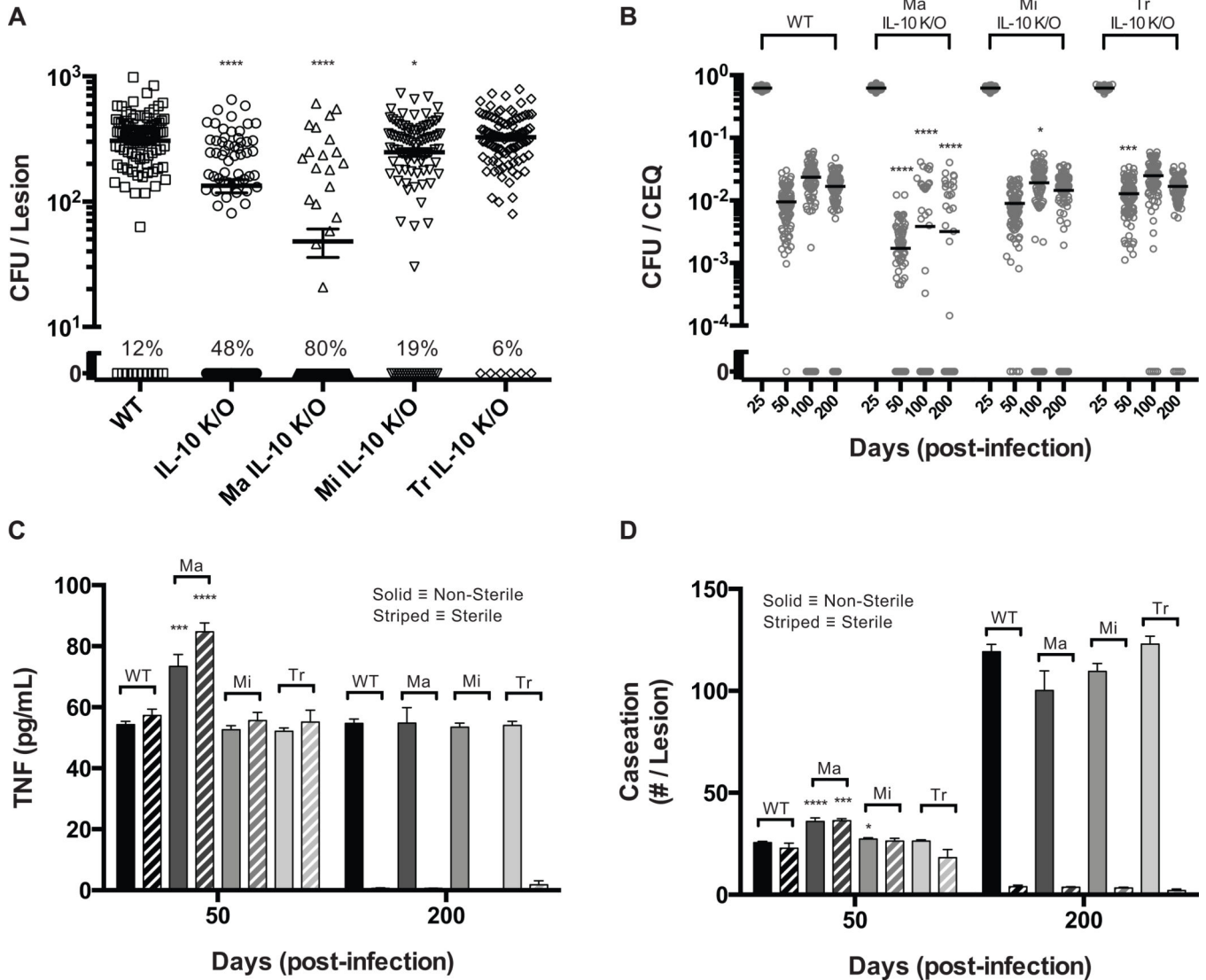
Figure 5. Virtual deletion of specific cellular sources of IL-10

A. CFU for WT, IL-10 K/O, activated macrophage IL-10 deletion (Ma IL-10 K/O), infected macrophage IL-10 deletion (Mi IL-10 K/O), regulatory T cell IL-10 deletion (Tr IL-10 K/O) lesions at 200 days post-infection. Both sterile and non-sterile lesions are included. The percentage indicates the number of sterile lesions at 200 days post-infection. B. CFU/CEQ for WT, IL-10 K/O, Ma IL-10 K/O, Mi IL-10 K/O, Tr IL-10 K/O lesions at 200 days post-infection. Both sterile and non-sterile lesions are included. C. Average TNF-α concentration for WT, Ma IL-10 K/O (Ma), Mi IL-10 K/O (Mi), Tr IL-10 K/O (Tr) lesions. Non-sterile lesions are displayed as solid bars and sterile lesions are displayed as striped bars. D. Caseous necrosis for WT, Ma IL-10 K/O (Ma), Mi IL-10 K/O (Mi), Tr IL-10 K/O (Tr) lesions. Non-sterile lesions are displayed as solid bars and sterile lesions are displayed as striped bars. Individual dots represent individual lesions. Lines indicate the mean values. Bars are representative of mean values with error bars showing SEM. For all panels: * p 0.05, ** p 0.01, *** p 0.001, **** p 0.0001, N = 100.
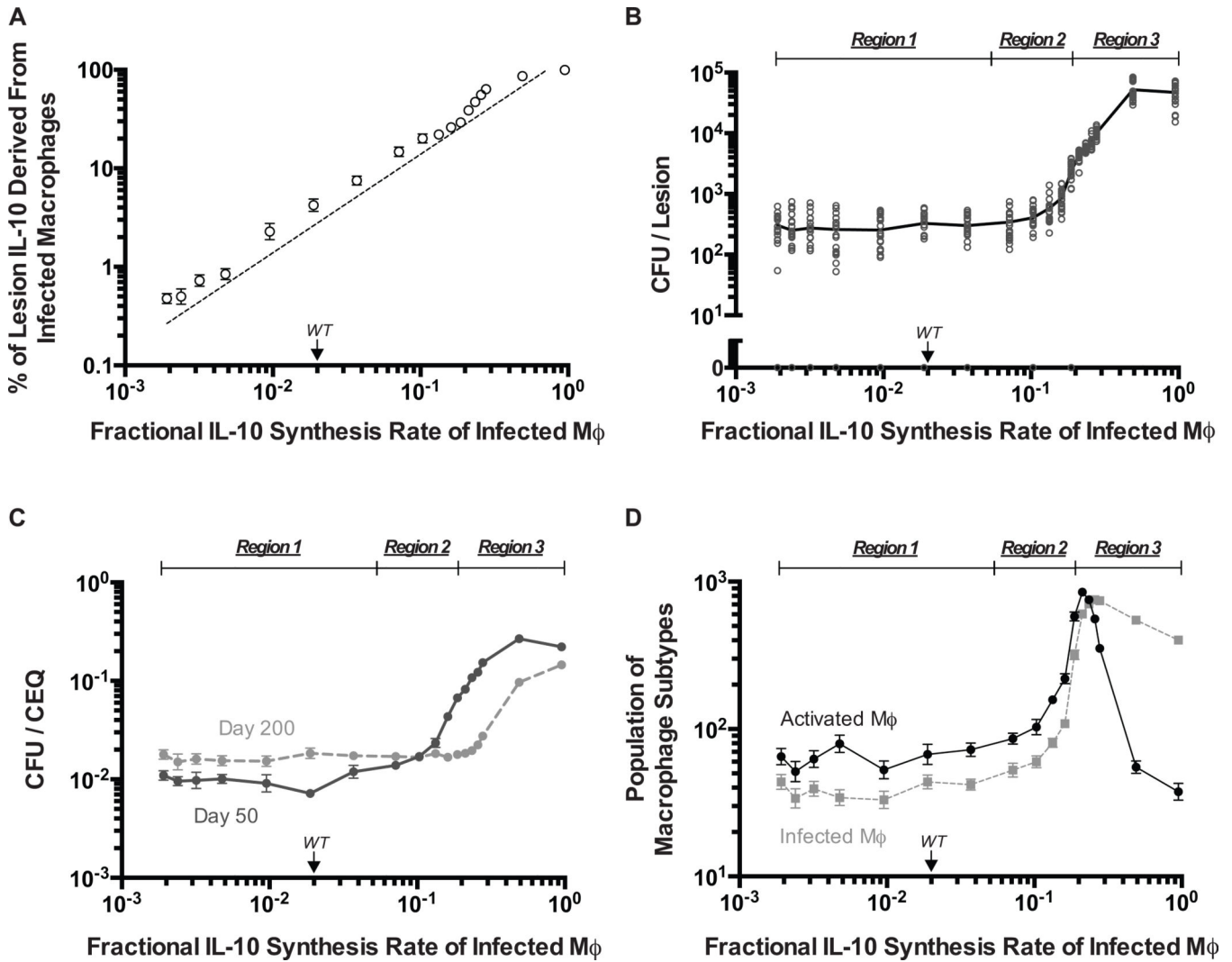
Figure 6. Infected macrophage derived IL-10 can undermine host-control of antimicrobial activity

A. Simulated percentage of IL-10 in the lesion at 200 days post-infection that is derived from infected macrophage IL-10 production is highly linearly correlated with infected macrophage IL-10 fractional synthesis (f_{Mi}) (Pearson's r = 0.9265, p < 0.0001). B. Simulated response in CFU at 200 days post-infection for varying levels of infected macrophage IL-10 fractional synthesis (f_{Mi}). C. Simulated response in CFU/CEQ at 200 days post-infection for varying levels of infected macrophage IL-10 fractional synthesis (f_{Mi}). D. Simulated response in macrophage populations at 200 days post-infection (activated macrophages – black circles, infected macrophages – grey squares) for varying levels of infected macrophage IL-10 fractional synthesis (f_{Mi}). For all panels: Region 1 (defined from fractional synthesis rates (f_{Mi}) of ~0.002 to ~0.05) represents the region where IL-10 is under the control of the host-response. Region 2 (defined from factional synthesis rates (f_{Mi}) of ~0.05 to ~0.2) represents the region of transitioning control of the IL-10 response. Region 3 (defined from factional synthesis rates (f_{Mi}) of ~0.2 to ~1.0) represents the region where IL-10 is under the control of the pathogen. Individual open dots represent

individual lesions. Solid dots indicate the mean values with error bars showing SEM. N = 20.
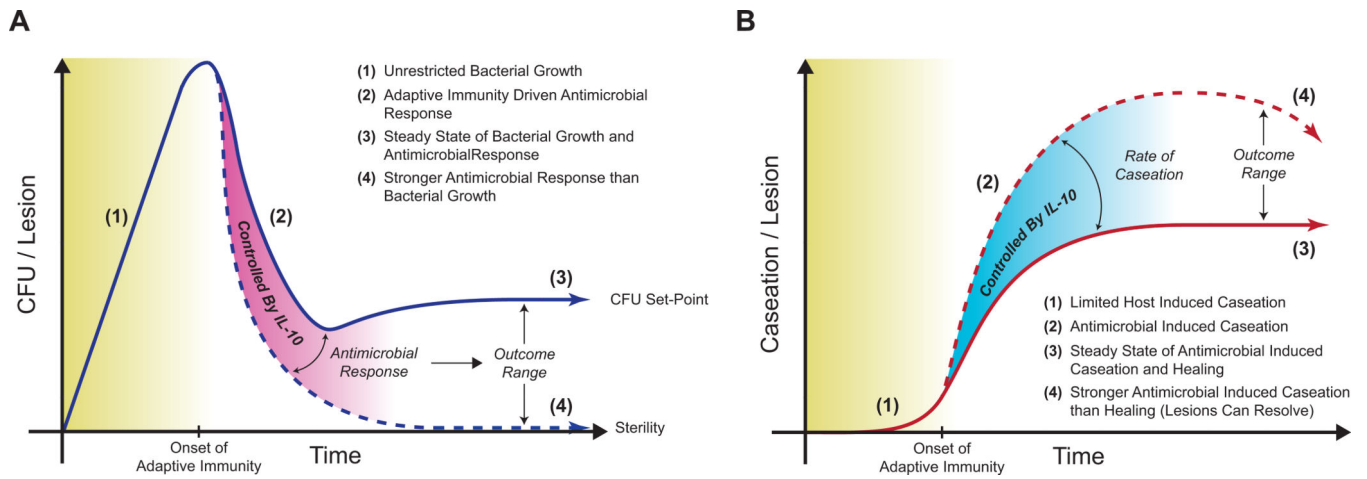
Figure 7. IL-10 controls sterility, bacterial set-point, and caseation on a per lesion basis
A. IL-10 control of bacterial dynamics in a lesion over time. B. IL-10 control of caseation in a lesion over time. The host antimicrobial response is controlled by IL-10. In non-sterile lesions, control antimicrobial responses by IL-10 leads to a bacterial set-point that balances bacterial replication with bactericidal processes, with minor caseation. Reducing IL-10 leads to increased antimicrobial responses, which promotes the lesion to sterilize at the cost of increased caseation. Lesions that sterilize may begin to resolve at later stages of infection (thus the downward slope of caseation), yet this could lead to fibrosis or scarring.

Table I

Median Instantaneous *Mtb* Doubling Times in Individual Lesions

Time (days post infection)	NHP Doubling Time[*] (1/days)	Model Doubling Time[+] (1/days)
10	1.83 (1.59 – 2.18)	1.73 (1.62 – 2.09)
20	1.87 (1.76 – 2.20)	2.09 (1.99 – 2.29)

Parentheses represent the minimum and maximum calculated doubling time for both NHP (N = 32) and ABM data (N = 100) sets

[*] Instantaneous doubling times estimated using median CEQ per lesion as defined in (52)

[+] Instantaneous doubling times estimated using CEQ per lesion and an exponential growth model defined from t(0) to t(t)